Thermal Reversion Mechanism of N-Functionalized Merocyanines to Spiropyrans: A Solvatochromic, Solvatokinetic, and Semiempirical Study

James T. C. Wojtyk,[†] Adnaan Wasey,[†] Peter M. Kazmaier,[‡] Shmaryahu Hoz,[§] and Erwin Buncel*,[†]

Department of Chemistry, Queen's University, Kingston, Ontario, Canada K7L 3N6, Xerox Research Center of Canada, 2660 Speakman Drive, Mississauga, Ontario, Canada L5K 2L1, and Department of Chemistry, Bar-Ilan University, Ramat-Gan 52100, Israel

Received: April 21, 2000; In Final Form: July 20, 2000

In continuing studies of the effect of solvent and molecular structure on the behavior of photochromic and thermochromic dye molecules, especially spiropyran (SP)−merocyanine (MC) interconversions, we have examined a series of 6′-nitrobenzoindolinospiropyrans (6-nitro-BIPS) with varying N-functionalities (R = CH_3, CH_2CH_2COOH, $CH_2CH_2CH_2SO_3^-$, CH_2CH_2COO-Cholesteryl). The solvent effect was assessed by following the thermal decay of the photochemically ring-opened merocyanine to the spiropyran (MC ⇋ SP) via UV/vis spectroscopy at the λ_{max} of the MC form. It was found that while modification of the N-moiety produced no perturbations in the solvatochromic behavior of these dyes, there was a marked effect on the solvatokinetic behavior. In nonpolar solvents, where the MCs possess predominantly quinoid character (unit central bond order), a constant thermal reversion rate was observed for the MCs with electron-rich N-ligands. This was attributed to electronic and steric interactions between the ligands and the phenoxide moiety. However, in polar solvents the increased zwitterionic character of the MCs (central bond order ∼2) leads to inhibition of the thermal reversion rate for the MCs in this study, independent of N-functionality. The MC ⇋ SP interconversion has also been examined by means of semiempirical calculations. These reveal the lowest energy pathway for conversion of the *trans*-MC to a *cis*-MC form via sequential bond rotation of the three central dihedral angles (α, β, and γ). The calculations support the observed solvatokinetic behavior, leading to the assignment of the *trans/cis* thermal isomerization as the rate-determining step in the overall process.

Introduction

Since the discovery of the photochromic properties of spiropyrans in 1952,[1] the spiropyran−merocyanine interconversion has been investigated for various applications, such as recording, copying, emissive displays, and, more recently, optical data storage and sensors.[2] Most commonly studied has been the *N*-methyl-6′-nitrobenzoindolinospiropyran (6-nitro-BIPS), SP-I ⇌ MC-I system:

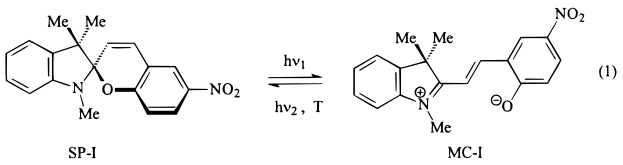

SP-I MC-I (1)

Our own interest in these systems is from the viewpoint of a photochemical binary element in optical data storage.[3] The basis of these molecular switches is that solutions of SPs are generally colorless (λ_{SP} = 200−400 nm), being composed of two heterocyclic rings linked by a common tetrahedral sp^3 carbon atom which enforces an orthogonal orientation between the two heterocycles. However, absorption of radiation in the SP absorption envelope leads to cleavage of the C−O bond and ring-opening to produce the merocyanine (MC). Upon ring opening, the previously isolated halves of the molecule form a planar structure that allows for π-orbital overlap, shifting λ_{max} to the visible region (540−580 nm). The open form generally adopts a *trans* structure that is more stable than the *cis* form as it minimizes nonbonding interactions. Thus, the initially colorless solutions of spiropyrans upon exposure to UV radiation become deeply colored on formation of the merocyanine. The colored merocyanine solutions revert either thermally to the spiropyran state following a first-order kinetic rate law, or photochemically.[4] Indeed, the extensive amount of research conducted on this photochromic system has led to a prototypical device capable of storing information, based on doping the SPs into a PMMA polymer.[4,5]

The thermal reversion pathway to re-form the SP generally occurs spontaneously at ordinary temperatures, precluding application to optical data storage systems. Hence, studies are being conducted to develop SPs that do not revert thermally at room temperature. Our own approach has recently been to design and develop a molecular switch based on photochromic spiropyrans that are capable of selectively chelating a divalent metal in the MC form, thereby stabilizing the colored species.

We recently reported our work toward the development of a molecular switch that inhibits the thermal reversion process through attachment of a chelating ligand onto a 6′-nitro-SP as an *N*-indolino substituent.[6] Photoirradiation of these SPs results in heterolytic cleavage of the C−O bond, generating a bidentate MC ligand composed of the phenoxide and the *N*-indolino substituent. In the presence of a divalent metal ion, chelation

[†] Queen's University.
[‡] Xerox Research Center of Canada.
[§] Bar-Ilan University.

10.1021/jp001533x CCC: $19.00
Published on Web 09/07/2000

of the metal with the MC ligand preferentially stabilizes the MC complex from thermal reversion.[6]

A number of unsolved problems remain concerning the MC ⇌ SP transformation: the intimate structure of the photochemically produced colored species; the nature of any reaction intermediates; and the detailed mechanistic processes involved in the thermally reversible pathway between SP and MC. Semiempirical calculations have been reported on the ring-opened rotational isomers of 6-nitro-BIPS to determine the most stable *trans*-MC form and the different *trans*-conformers involved in the overall thermal cyclization reaction mechanism.[7] In other studies, dynamic NMR and NOE experiments have been performed on ring-opened systems to determine the most stable conformer.[8] Investigations by transient nanosecond and picosecond spectroscopy[9a,b] and laser flash photolysis[9c] have led to the observation of the high-energy *cis*-form as a transient intermediate. A number of linear free energy relationships (LFERs) have been developed to examine the mechanisms and intermediates of ring closure.[10]

Study of the thermal reversion of N-functionalized compounds offered a test of our hypothesis that electron-rich moieties would give rise to an inhibiting effect on the rate of the MC → SP thermal reversion. This will arise from the electrostatic interactions between the ligand and the phenoxide moiety, precluding the nucleophilic attack of phenoxide that re-forms the *spiro* ring. In the present study of spiropyrans II−IV, the solvent dependence of the thermal reversion rate and absorption maximum has been examined via UV/vis spectrophotometry and compared to that of SP-I. The study sheds light on the effect of N-substituent modification on the ring closure mechanism and electronic distribution of the MC.

SP-I−III and a novel SP, the cholesteryl ester derivative, SP-IV, were investigated to examine electrostatic, inductive, and steric effects on ring closure. To complement the solvent effect

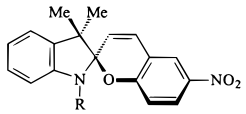

SP	R
I	CH_3
II	$(CH_2)_2COOH$
III	$(CH_2)_3SO_3^-NHEt_3$
IV	$(CH_2)_2COO$-cholesteryl

study, the ring closure mechanism has been analyzed via molecular modeling. In light of the earlier studies reporting experimental observation of the *cis*-MC as a transient intermediate,[9] the *trans*-MC → *cis*-MC isomerization has been examined through rotation about the three central dihedral angles. This has shed light on the number of steps and the order in which they occur sequentially for ring closure. The results enhance our understanding of the effects of N-substituents and solvent effects and have allowed us to elucidate the lowest energy pathway of the MC → SP conversion, incorporating the *cis*- as well as the *trans*-MC forms.

Experimental Section

Synthesis and Procedure. The synthesis of SP-I−III used in this study has been reported previously in the literature.[2,6,11] SP-IV was synthesized via *N*,*N*′-dicyclohexylcarbodiimide (DCC)/*p*-(dimethylamino)pyridine (DMAP) coupling of SP-II with cholesterol in THF.

Synthesis of SP-IV. Into a 100-mL round-bottomed flask equipped with a pressure-equalized dropping funnel, a magnetic stirring bar, and an argon inlet were added SP-II (0.574 g, 1 mmol) and cholesterol (0.353 g, 1 mmol). After they were dissolved in dry THF (10 mL) and cooled to 0 °C, a solution of DCC (0.314 g, 1.62 mmol) and DMAP (0.042 g, 0.35 mmol) in THF (4 mL) was added dropwise over 45 min. The mixture was stirred at 0 °C for a further 2 h and then gradually warmed to 25 °C over 12 h. During the warming period, a dicyclohexylurea (DCU) precipitate formed which was filtered and washed with THF (3 × 50 mL). The filtrate was evaporated under reduced pressure to give a red/purple precipitate. Flash chromatography ($CHCl_3$:silica gel) gave yellow crystals of SP-IV in 36% yield, mp 212−213 °C. Anal. Calcd for $C_{48}H_{64}O_5N_2$: C, 76.97; H, 8.55; N, 3.74. Found: C, 77.19; H, 8.43; N, 3.68.

^{1}H NMR (400.1 MHz) in DMSO-d_6: δ 8.04 (1H, d), 8.03 (1H, s), 7.28 (1H, s), 7.22 (1H, t), 7.11 (1H, d), 6.93 (2H, m), 6.77 (1H, d), 6.64 (1H, d), 5.89 (1H, d, J = 10.5), 5.36 (1H, m), 4.55 (1H, m), 3.58 (2H, m), 2.62 (2H, m), 2.32 (2H, d), 2.0−0.8 (43H, m), 0.72 (3H, s).

^{13}C NMR (100.1 MHz) in DMSO-d_6: 171.3, 159.5, 146.9, 141.3, 139.4, 136.5, 128.3, 127.7, 125.8, 122.8, 122.0, 121.6, 119.7, 118.5, 115.5, 106.5, 105.7, 74.4, 56.7, 56.1, 52.9, 50.0, 42.3, 39.7, 39.5, 39.3, 38.1, 36.9, 36.3, 36.1, 35.8, 34.0, 31.9, 31.4, 28.3, 28.0, 27.7, 25.8, 24.3, 23.8, 22.6, 22.4, 21.0, 19.8, 19.3, 18.7, 11.8.

IR (KBr, cm^{-1}): 2943, 2866, 1730, 1654, 1611, 1577, 1514, 1483, 1337, 1270, 1180, 1090, 1020, 951, 915, 800.

UV/vis (λ_{max}, ϵ): 342 nm, 12 000 M^{-1} cm^{-1}.

Spectrophotometric Method. All glassware was washed with ethanol and acetone and soaked in an acid bath (2 M HCl) for 24 h before being dried under vacuum at 150 °C. Solvents purified on a bulk scale for this study were DMSO, acetone, DMF, and acetonitrile using literature procedures.[12] Additional organic solvents used in this study were of spectrophotometric grade (Aldrich, Sure-Seal) and were used as supplied. The solvents used in the study include toluene, diethyl ether, tetrahydrofuran, 1,4-dioxane, acetone, *N*,*N*-dimethylformamide, ethanol, and water.

Stock solutions of SPs (1 × 10^{-2} M) in DMSO or DMF were made up in 5-mL volumetric flasks in an inert atmosphere, and then the flasks were capped with a rubber septum, wrapped in aluminum foil, and stored at 0 °C. The physical properties associated with each spiropyran are listed in Table 1.

Reproducible results of the photochromic transformation of spiropyran to merocyanine were obtained through development of a protocol that maximized formation of the colored form. Briefly, 2.00 mL of the selected organic solvent was injected into a 1.0-cm-path length quartz cuvette via a 2.5-mL syringe, and then the cuvette was capped with a Teflon plug and placed into the thermostated (25 °C) cell compartment of a HP 8452 diode array spectrophotometer which was covered with a metal lid to preclude exposure to ambient light. The "blank" spectrum was acquired, and then a 10-μL aliquot of the spiropyran stock solution in DMF or DMSO was injected into the cuvette ([SP] = 5 × 10^{-5} M). Within the concentration range of (1−10) × 10^{-5} M, the absorption intensities of SP and MC followed Beer's law. The cuvette was placed in a SpectroLine ultraviolet irradiation chamber equipped with two 15-W long-wavelength (365 nm) tubes and irradiated with 365-nm light for 90 s to obtain the maximum concentration of the colored MC form. The cuvette was then transferred immediately to the cell compartment of the spectrophotometer, and absorption spectra were acquired at constant time intervals to follow the merocyanine decay. The reaction was followed for 10 half-lives, and the scanning rate was at intervals that allowed approximately 10 data points per half-life (Figure 1).

The observed rate constant (k_{obs}) is the sum of the two rate processes, k_1 and k_2:

TABLE 1: Effect of Solvent on the Absorption Maximum (λ_{max}) and the Observed Rate Constants (k_{obs}) for Thermal Reversion of MC-I, II, III, and IV to the SP Forms at 25 °C.

		MC-I		MC-II		MC-III		MC-IV	
solvent	$E_T(30)$[a]	λ_{max} (nm)	k_{obs} (10^3 s^{-1})	λ_{max} (nm)	k_{obs} (10^3 s^{-1})	λ_{max} (nm)	k_{obs} (10^3 s^{-1})	λ_{max} (nm)	k_{obs} (10^3 s^{-1})
toluene	33.9	600	122	604	54.8	596	12.2	608	47.5
Et_2O	34.6	594	103	596	42.8	nr[b]	nr	600	47.3
1,4-dioxane	36.0	590	63.9	594	50.2	584	18.9	594	45.4
THF	37.4	584	26.8	590	48.9	582	12.2	590	52.5
acetone	42.2	568	7.28	574	20.0	568	3.38	574	32.7
DMF	43.8	562	2.85	564	4.45	566	1.27	570	5.45
EtOH	51.9	540	0.69	548	0.60	546	0.66	546	0.66
H_2O	54.0	nr[b]	nr[b]	506	~0[c]	508	~0[c]	nr[b]	nr[b]

[a] $E_T(30)$ is Reichardt's empirical solvent polarity parameter.[18] [b] Ring-opening to the merocyanine form was not observed in these solvents. [c] Thermal reversion was not observed over the 3-day monitoring period.

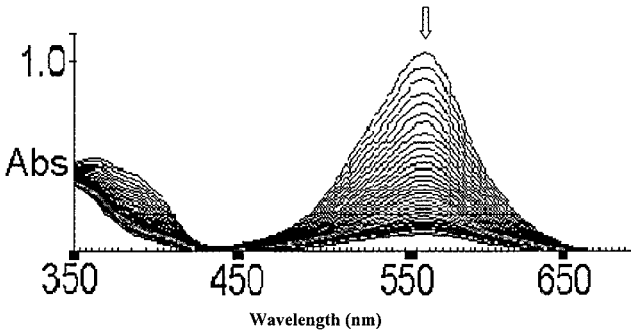

Figure 1. Overlay spectra at 10-s intervals to monitor the thermal decay of MC-I (λ_{max} = 568 nm, [MC-I] = 5×10^{-5}M) in acetone at 298 K (total acquisition time = 900 s).

$$SP \underset{k_2}{\overset{k_1}{\rightleftharpoons}} MC$$

The SP → MC thermal ring-opening process can be ignored, i.e., $k_2 \gg k_1$. Observed rate constants (k_{obs}) for the thermal MC → SP reversion were calculated over three half-lives using the equation derived from the first-order rate law ($-dA/dt = k_{obs}A$) and converted to a common logarithmic value,

$$\ln(A_t - A_{inf}) = -k_{obs}t + \ln(A_o - A_{inf})$$

where A_o, A_t, and A_{inf} are the absorbances at times 0 and t and after 10 half-lives, respectively. Linear regression of this equation provided the observed rate constants (k_{obs} = $-2.303 \times$ slope) and correlation coefficients (R^2 values). This standard protocol was performed in triplicate to obtain rate constants within ±5% ($R^2 > 0.999$). Values quoted are average values.

Semiempirical Calculations. All semiempirical calculations were carried out at the restricted Hartree−Fock (RHF) level with the MNDO-PM3 SCF-MO method,[13] as implemented in the Spartan 3.0 program.[14] The three central dihedral (torsional) angles between the indolenine and the phenoxide moieties were labeled α, β, and γ.

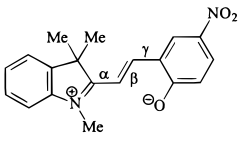

The most stable conformers of the *trans*-MC and *cis*-MC forms were determined by geometric optimization with the β dihedral constrained to 180° for the *trans*-MC (α = 180, β = 180, γ = 180) and 0° for the *cis*-MC (α = 90, β = 0, γ = 0).

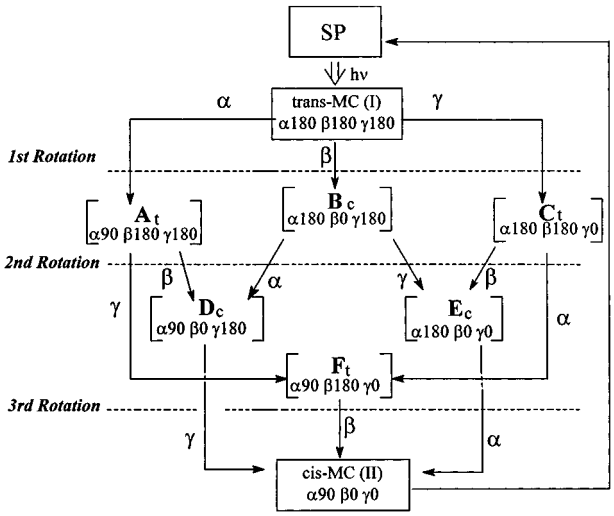

Figure 2. Schematic depiction of dihedral rotation combinations, α, β, and γ, for transformation from *trans*-MC (I), α180, β180, γ180, to *cis*-MC (II), α90, β0, γ0.

These two conformations were the boundary conditions or the lowest energy ground states in the overall *trans* → *cis* isomerization.

The conversion from *trans*-MC to *cis*-MC involves rotation about each of three dihedral angles. To determine the rotation sequences, the flowchart in Figure 2 was followed in the conversion from *trans*-MC to *cis*-MC. Calculation of the rotational barrier for each dihedral rotation involved geometrical optimization of each conformer formed after rotation about the dihedral in 15° increments while the other two dihedrals were constrained. Overall, the α dihedral was rotated from 180 → 90°, while the β and γ dihedrals were rotated from 180 → 0°. The calculations afforded the heats of formation, ΔH_f (kcal/mol), for each conformer in the rotation process. A plot of ΔH_f versus the bond angle rotation afforded the barrier to rotation for each dihedral. The geometry and ΔH_f value at the potential energy maximum for each dihedral rotation were further confirmed by calculation of the first-order saddle point along the reaction coordinate, i.e., the structure with one imaginary vibrational frequency, using the transition-state search algorithm in Spartan 3.0. The results (Table 1S, Supporting Information) are in satisfactory agreement with those reported herein.

Results

Solvent Effect Study. The effect of solvent on the thermal decay rate of functionalized merocyanines obtained on irradiation of the spiropyran was examined spectrophotometrically using the protocol described in the previous section. The

TABLE 2: Heats of Formation (H_f) and Barriers for Rotation about the α, β, and γ Dihedrals in the Most Stable *trans*-MC (I) Conformer, α180 β180 γ180, To Generate Conformers A_t, B_c, and C_t: First Bond Rotation

initial geometry	H_f^i (kcal/mol)	ϕ	barrier (kcal/mol)	H_f^f (kcal/mol)	final geometry
α180, β180, γ180 (I)	9.8	α(180 → 90)	22.6	32.4	α90, β180, γ180 (**A_t**)
		β(180 → 0)	30.7	40.5	α180, β0, γ180 (**B_c**)
		γ(180 → 0)	24.3	10.2	α180, β180, γ0 (**C_t**)

TABLE 3: Heats of Formation (H_f) and Barriers to Rotation Following the Second Series of Rotations for Conformers A_t, B_c, and C_t about the α, β, and γ Dihedrals To Form Conformers D_c, E_c, and F_t: Second Bond Rotation

initial geometry	H_f^i (kcal/mol)	ϕ	barrier (kcal/mol)	H_f^f (kcal/mol)	final geometry
α90, β180, γ180 (**A_t**)	32.4	γ(180 → 0)	1.5	32.2	α90, β180, γ0 (**F_t**)
		β(180 → 0)	26.3	33.6	α90, β0, γ180 (**D_c**)
α180, β0, γ180 (**B_c**)	40.5	α(180 → 90)	(−7.3)		
		γ(180 → 0)	8.5	40.1	α180, β0, γ0 (**E_c**)
α180, β180, γ0 (**C_t**)	10.2	β(180 → 0)	29.9		
		α(180 → 90)	22.5	32.2	α90, β180, γ0 (**F_t**)

TABLE 4: Heats of Formation (H_f) and Barriers to Rotation Following the Rotations of α, β, and γ in Conformers D_c, E_c, and F_t To Form the Most Stable *cis*-MC Conformer (II), α90, β0, γ0: Third Bond Rotation

initial geometry	H_f^i (kcal/mol)	$\phi_{rotated}$	barrier (kcal/mol)	H_f^f (kcal/mol)	final geometry
α90, β0, γ180 (**D_c**)	33.6	γ(180 → 0)	1.5		
α180, β0, γ0 (**E_c**)	40.1	α(180 → 0)	(−7.5)	32.7	α90, β0, γ0 (II)
α90, β180, γ0 (**F_t**)	32.2	β(180 → 0)	32.4		

observed spectrophotometric data and derived first-order rate constants for the MC → SP reversion in the solvents toluene, diethyl ether, THF, 1,4-dioxane, acetone, DMF, and EtOH are listed in Table 1. The solvatochromic and solvatokinetic data for MC-I have been reported previously.[15]

The data presented in Table 1 show that the absorption properties and the rates of thermal reversion are, indeed, solvent dependent. For all of the merocyanines, a hypsochromic shift of the absorption maximum is observed as the polarity of the solvent increases. The rate of the thermal reversion, from the merocyanines to the spiropyrans, also decreases as the solvent polarity is increased. For MC-I, an inverse relationship between the solvent polarity and the rate of thermal decay is observed: there is a steady decrease in k_{obs} values (0.122 s^{-1} → 0.0268 s^{-1}) on increasing the polarity of the medium from toluene to THF. However, for the N-functionalized merocyanines II−IV, in solvents of nonpolar character (i.e., toluene, diethyl ether, THF and 1,4-dioxane), the k_{obs} values remain constant at 0.048, 0.014, and 0.047 s^{-1}, respectively. In more polar solvents, beginning with acetone, there is a decrease in the k_{obs} values, similar to the observation for MC-I, with rates converging in EtOH, i.e., $k_{obs} \approx 6.5 \times 10^{-4}$ s^{-1} for all the MCs.

Semiempirical Calculations. Theoretical calculations have been performed to determine the order of sequential dihedral bond rotations and the lowest energy pathway in the thermal reversion of *trans*-MC (I) to *cis*-MC (II), as the immediate precursor of the ring-closed SP form. As illustrated in Figure 2, three rotations are required to convert the *trans*-MC to the *cis*-MC form. Rotation about each of three dihedral (torsional) angles in 15° increments while constraining the other two made it possible to calculate the barrier to rotation about each bond. The rotations (ϕ) examined for each dihedral are α(180 → 90), β(180 → 0), and γ(180 → 0). The various possible permutations involving α, β, and γ, and the resulting enthalpies and barriers to rotation for the transformation *trans*-MC → *cis*-MC, are shown in Tables 2−4 in terms of the dihedral angles during bond rotation.

Geometric optimization on the ground-state forms of SP, *cis*-MC (α90, β0, γ0) and *trans*-MC (α180, β180, γ180) gave heats of formation, relative to the SP form, of 0, 9.8, and 32.7 kcal/mol, respectively.

First Bond Rotation. Beginning with the most stable *trans*-MC conformer, I, the first series of dihedral rotations (ϕ) involve each of the α, β, and γ dihedrals (Figure 2). In Table 2, the calculated values of barriers to rotation and the heats of formation are given for the initial and final geometries. Rotation of the α dihedral (180 → 90) is associated with a barrier of 22.6 kcal/mol and an increase in energy to 32.4 kcal/mol for conversion of *trans*-MC (I) to the *trans* conformer denoted as **A_t**. The highest rotation barrier (30.7 kcal/mol) is observed for the β dihedral (180 → 0) in the *trans* → *cis* isomerization, which also results in the *cis* conformer **B_c** having the highest energy, 40.5 kcal/mol. Rotation of the γ dihedral (180 → 0, 24.3 kcal/mol) is similar energetically to α rotation, the energy change to conformer **C_t** being minimal, 0.4 kcal/mol.

Second Bond Rotation. The conformers **A_t**, **B_c**, and **C_t** formed from the first bond rotation can each undergo two dihedral rotations, as depicted by Figure 2. In Table 3 are listed the barriers to rotation and the heats of formation for the initial and final geometries, **D_c**, **E_c**, and **F_t**.

Rotation of the γ dihedral in conformer **A_t** to form conformer **F_t** is associated with a small barrier of 1.5 kcal/mol, and a negligible change in enthalpy. However, while rotation of the β dihedral on going from **A_t** to **D_c** does not alter the enthalpy of the system (Table 3), the barrier in forming conformer **D_c** is 26.3 kcal/mol.

Rotation of the α dihedral in the **B_t** conformer to form **D_c** shows no barrier to rotation and a decrease in enthalpy of 7.3 kcal/mol. Furthermore, rotation of the γ dihedral to form conformer **E_c** results in a minimal change in energy with a barrier of 8.5 kcal/mol (Table 3).

For conformer **C_t**, rotation of the α dihedral to form conformer **F_t** is associated with a large barrier of 22.5 kcal/mol and an increase in the enthalpy of the system of 22.0 kcal/mol. The *trans* → *cis* isomerization, **C_t** → **E_c** (β:180 → 0), also required a large barrier, and the enthalpy increase was 29.9 kcal/mol (Table 3).

Third Bond Rotation. The last dihedral rotations to form the most stable *cis*-MC conformer, II, involve rotation about each of the α, β, and γ dihedrals in conformers **D_c**, **E_c**, and **F_t**. In Table 4 are given the respective barriers to rotation and the heats of formation for **D_c**, **E_c**, **F_t**, and *cis*-MC (II). Conformer **D_c** has

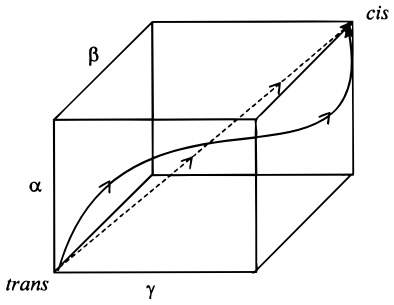

Figure 3. Diagram illustrating different possible pathways in isomerization of *trans*-MC (I) to *cis*-MC (II) conformer: along axes of cube (e.g., α, β, γ, in sequence); fully concerted pathway (- - -); and one of the possible nonconcerted pathways (solid curve).

a heat of formation of 33.6 kcal/mol; 180° → 90° rotation of the γ dihedral to form the most stable *cis*-MC conformer is subject to a minimal barrier to rotation (1.5 kcal/mol) with a small decrease in enthalpy (0.9 kcal/mol). The dihedral rotations for $\mathbf{F_t}$ and $\mathbf{D_c}$ led to minimal changes in the enthalpy. However, the β dihedral rotation of $\mathbf{F_t}$ → *cis*-MC (II) corresponds to *trans*/*cis* isomerization and has a large barrier to rotation of 32.4 kcal/mol. In contrast to this, α rotation of $\mathbf{E_c}$ to form *cis*-MC (II) is associated with no barrier and a 7.5 kcal/mol decrease in enthalpy (Table 4).

The computational studies described are for stepwise processes in the conversion of *trans*-MC (I) to *cis*-MC (II). However, the representation in Figure 3 suggests that many other pathways could be followed in isomerization from the *trans* to the *cis* conformer. In this diagram (a 3-D version of the More-O'Ferrall−Jencks diagrams),[16] each of the axes represents a dihedral angle; our calculations followed a stepwise pathway with no deviation from the axes. In contrast, the dashed line traversing from the lower left to the upper right corner pertains to a fully concerted mechanism. As hybrids of these two extremes, there are many possibilities that encompass both the stepwise and the concerted mechanisms, for which computational modeling is not attempted in the present study.

Discussion

1. Solvatochromic Behavior. Merocyanine dye molecules have electronic structures that lie between the polyenes and polymethines, depending on the nature of the heteroatoms and solvent polarity.[17] Merocyanines are comprised of an electron-donating group, D, linked through a π-conjugated species to an electron-accepting group, A, and can be described in terms of two mesomeric structures: D−R═A ↔ D^+═R−A^-. The electronic transition from the chromophore is an intramolecular charge transfer between the donor and acceptor groups, generating an excited state with a dipole moment (μ_e) that is appreciably different from the ground-state dipole moment (μ_g).

We have observed very pronounced solvent effects on the spectral characteristics of merocyanines I−IV; these result from a change in the dipole moment upon electronic excitation. Plots of the wavenumber (ν, cm^{-1}) versus the $E_T(30)$ parameter[18] for all MCs (Figure 4) examined exhibit negative solvatochromism, i.e., λ_{max} decreases with an increase in the solvent parameter $E_T(30)$, in accordance with the ground state being more dipolar than the excited state ($\mu_g > \mu_e$). Moreover, the solvatochromic behaviors of the various N-functionalized MCs are identical; i.e., the effects of solvent on μ_g and μ_e along the series of MCs are identical. Since these compounds differ only in the nature of the N-ligand, it follows that the solvatochromism is not affected by the nature of the N-substituent. *Thus, attachment of a chelating moiety on the N-indolino portion of SP does not affect the dipole moments of the ground state or the excited state. It can hence be concluded that the electronic structure of the merocyanine is determined solely by the solvent medium and is independent of the N-substituents used in this study.*

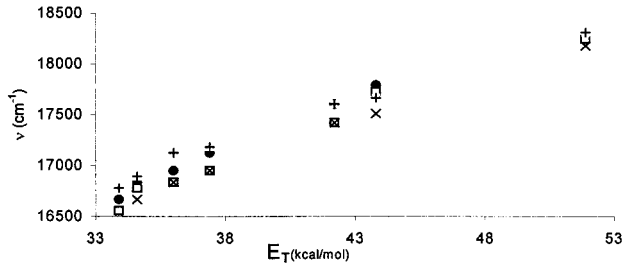

Figure 4. Plots depicting the similar solvatochromic behavior of MC-I (●), MC-II (□), MC-III (+), and MC-IV (×),1.0 × 10^{-4} M, at 25 °C.

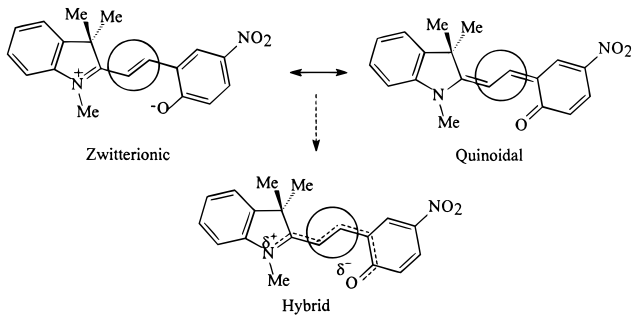

Figure 5. Illustrations of the zwitterionic, quinoidal, and hybrid structures of MC-I as affected by solvent polarity. The critical double/single bond which is affected by solvent polarity is circled.

To summarize, the N-functionalized MCs constitute a conjugated system that exhibits solvatochromism due to varying relative contributions of two canonical forms: nonpolar quinoidal and dipolar zwitterionic (Figure 5). These molecules exhibit a negative solvatochromic effect which is indicative of (a) a decrease in the dipole moment upon electronic excitation and (b) a concurrent increase in the ground-state dipole moment due to greater contribution of the zwitterionic mesomer. Moreover, since the solvatochromic behaviors of MC-I −IV are identical, it follows that both of these properties are independent of the nature of the N-substituent.

2. Mesomer-Dependent Ring Closure Mechanism. The mechanism for the thermal reversion of a *trans*-merocyanine to the spiropyran must involve a minimum of two steps: (1) *trans*−*cis* isomerization about the central double bond; and (2) a mesomer-dependent reaction to re-form the heterocyclic spiro ring. The first step results in conversion of the more thermodynamically stable *trans*-MC to a strained *cis*-MC geometry. The lifetime of the *cis*-MC species will be short due to the increase in strain energy arising from steric repulsions and conformational restriction. However, formation of the strained *cis*-MC brings the phenolate nucleophile into close proximity to the electron-deficient spiro carbon center (C_{spiro}), facilitating intramolecular reaction to re-form the more stable spiro ring system.

As shown by the solvatochromic data, dipole moments of the MCs change markedly with solvent polarity. In highly polar solvents, the visible absorption is shifted to higher energies relative to nonpolar solvents, i.e., a hypsochromic effect, contrasting with the xanthene dye Rhodamine B, which is stabilized only by protic solvents.[19] In the present system, this is due to the change in the relative contribution of the two

mesomeric structures that comprise the overall MC form, quinoidal and zwitterionic (Figure 5), toward the latter structure. The bond orders in the mesomers differ, in particular the central β bond, which has to undergo a *trans* → *cis* isomerization along the reaction coordinate to re-form the SP.

Conversion of the *cis*-MC to SP in solvents where the quinoidal form of the MC predominates can be formulated as an intramolecular electrocyclic process via the transition state (**TS***).[20] These types of reactions do not have an appreciable

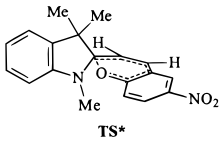

TS*

solvent dependency associated with them,[21] which argues against this being the rate-determining step (RDS), noting the marked solvent effect which is observed on the rate of ring closure.

On the other hand, in the zwitterionic form, the ring closure mechanism can be likened to an anion−cation recombination reaction. Ritchie has studied extensively the effect of solvent on the rates of recombination of carbocations and some other electrophiles with anionic and neutral nucleophiles.[22] The carbocations used were typically tropylium, trityl, and xanthylium, while nucleophiles were typically thiolate, cyanide, and free amines. However, no spectacular solvent effect on rates and equilibria was found over the range acetone → water. This can be explained on the basis of a balancing solvent effect on cation stabilization and anion destabilization in these systems. Furthermore, Hoz et al.[23] highlighted the importance of the electrophile LUMO in studies of nucleophilic attacks on low-LUMO substrates. The significant solvatochromic behavior observed in the present work shows that the ground state is being stabilized by the solvent. However, since the LUMO remains essentially constant with solvent change, if the recombination reaction contributed to the rate-determining step of the reversion then no solvent effect would be observed for the thermal reversion. Thus, the observation of a significant solvent effect would rule out cation−anion recombination as the RDS step of MC → SP ring closure.

Increasing the solvent polarity stabilizes the zwitterionic mesomeric form over quinoidal of *trans*-MC in the ground state, concomitant with an increase in bond order of the central C−C bond circled in Figure 5. The will result in a decrease in the rate of isomerization, *trans*→ cis, noting that the barrier to rotation for a typical C═C bond is ∼65 kcal/mol, while for C−C it is very much lower, ∼5 kcal/mol. It follows that a *trans*-MC with high zwitterionic character will have associated a large energy barrier to isomerization to the *cis*-MC form and that the extent of zwitterionic character will be solvent dependent.

3. Solvatokinetic Behavior. The solvatokinetic behavior of MC-I was examined by Keum et al., who found a linear correlation between the thermal reversion rate and $E_T(30)$, an increase in the polarity of the medium resulting in a decrease of the thermal reversion rate.[15] Moreover, the decrease of the thermal reversion rate was dependent on the extent of zwitterionic character of the *trans*-MC-I, as measured by the solvatochromic absorption maximum shift, i.e., the λ_{max} and k_{obs} values and solvent polarity were codependent, in agreement with the above discussion.

While the solvatochromic behaviors, i.e., solvent effects on the absorption maxima, of MCs in this study are closely similar and follow a linear trend in the plot of ν (cm^{-1}) versus $E_T(30)$ (Figure 4), the solvatokinetic behaviors differ along the series.

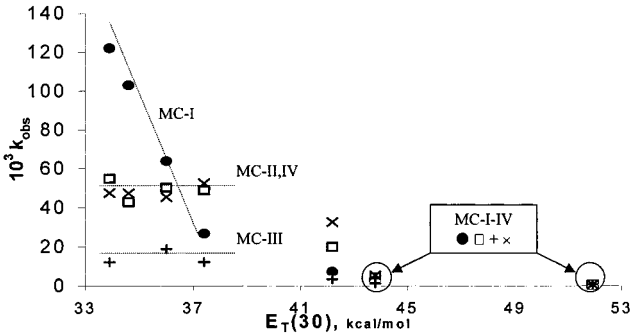

Figure 6. Plot of the observed rate constants for the thermal reversion of MC-I (●), MC-II (□), MC-III (+), and MC-IV (×) in solvents of varying polarity as a function of the $E_T(30)$ parameter.

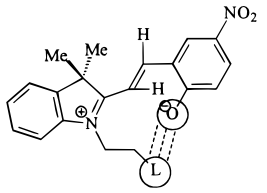

Figure 7. Illustration of the electrostatic repulsions between the ligand (L) and the aryloxide moiety in the proposed transition structure of the rate-determining step for the overall thermal reversion of *trans*-MC to SP.

As shown in Figure 6, the plots of k_{obs} versus $E_T(30)$ for the thermal reversion of MC-II−IV differ from that of MC-I. Unlike MC-I, which shows an inverse relationship between k_{obs} and $E_T(30)$, in the case of MC-II−IV the plot can be dissected into two distinct regions. The first region is a plateau corresponding to the nonpolar solvents used in the study, i.e., toluene, 1,4-dioxane, Et_2O, and THF, where the k_{obs} values remain virtually constant. However, in the second region, corresponding to the more polar solvents, i.e., acetone, DMF, and EtOH, there is a steady decrease in the k_{obs} values.

In the nonpolar solvents, the main contributor will be the quinoidal species in which the central bond has essentially unit bond order (Figure 5). Hence, rotation about this "single bond" to form the *cis*-MC (II) will be associated with a low barrier. The mechanism for ring closure of the quinoidal form will be an electrocyclic process, as discussed previously, which will be associated with minimal solvent effect.[20]

In contrast, the main contributor in polar solvents will be the zwitterionic species, with the central bond having essentially a bond order of 2. Rotation about this (double) bond will be associated with a significantly larger barrier than for the quinoidal structure.

Considering the effect of substitution at the indolenine nitrogen by electron-rich ligands [$-(CH_2)_3SO_3^-$, $-(CH_2)_2$-COOH], it can be expected that electrostatic repulsions between these ligands and the oxygen of the aryloxide moiety would interfere with the orientation required for ring closure and thereby retard the rate of reversion to SP, as illustrated in Figure 7. The purely steric effect of the cholesterol substituent in MC-IV will be manifested similarly.

The effect of changing solvent, nonpolar → polar, is illustrated in Figure 8, which depicts the energetics for the transformations, *trans*-MC → *cis*-MC → SP. It follows from the previous discussion on the relationship between central bond order and solvent polarity that in nonpolar solvents, where the quinoid MC structure predominates and this bond order is unity, these N-substituents will exhibit a major rate-retarding effect. However, in highly polar solvents, where the zwitterionic structure is predominant, the effect of substituents will be marginal only.

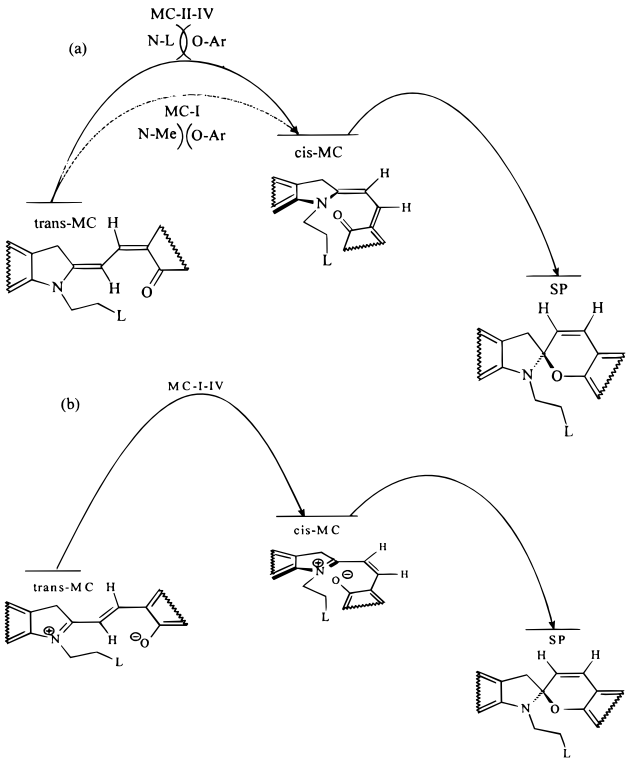

Figure 8. Potential energy−reaction coordinate diagram for conversion of MC → SP. (a) In nonpolar media (toluene → THF), where the quinoidal MC form is the major contributor with unit central bond order, the higher energy barrier for MC-II−IV (—) relative to that for MC-I (- - -) resulting from interaction of the N-functionality (N-L) and the Ar−O^- moiety. (b) In polar media (acetone → EtOH), due to the increase in zwitterionic contribution with double central bond order for MC-I−IV (—).

For nonpolar solvents, the energy barriers for the *trans*-MC → *cis*-MC isomerization (the RDS) will be higher with MC-II−IV than for MC-I due to steric interactions between the N-ligand and the aryloxide moiety, denoted as N-L)(OAr. As shown by the k_{obs} vs $E_T(30)$ plot in Figure 6, MCs II−IV exhibit a profile with a plateau in nonpolar solvents followed by a rate retardation, contrasting with the inverse relationship found between k_{obs} and $E_T(30)$ for MC-I. The relative constancy of the thermal reversion rates in nonpolar solvents for MC-II−IV signifies that the activation barriers emanating from the interaction between the N-substituent and the aryloxide moiety are unaffected by these solvents (Figure 8a).

In polar solvents (Figure 8b), the energy barrier corresponding to the RDS is no longer dependent on the interactions between the N-ligand and the phenoxide moiety. The dominant factor now is the essentially double bond nature of the central bond resulting from increased zwitterionic character with its accompanying high rotational barrier. Hence, there is no differentiation between MC-I through MC-IV, and the reaction profile in Figure 8b has coalesced to a single curve. This is reflected in the data of Figure 6, where the k_{obs} values for MC-II−IV are very similar to that of MC-I.

Ligand Electrostatic Effect. Attachment of chelating ligands, $(CH_2)_2COOH$ and $(CH_2)_3SO_3^-$, to the indolino nitrogen results in an increase in the electron density of the end groups for the N-functionalities of MC-II and MC-III relative to MC-I, as shown by the calculated atomic charges of the carboxyl and sulfonate groups using semiempirical methods (Spartan 3.0, PM3), Figure 9. The increase in electron density of the chelating moiety will give rise to through-space electrostatic repulsions between the ligand and the phenolate moiety. These repulsive

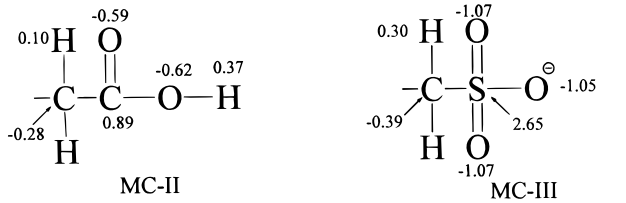

Figure 9. Calculated atomic charges on N-ligands in MC-II−III.

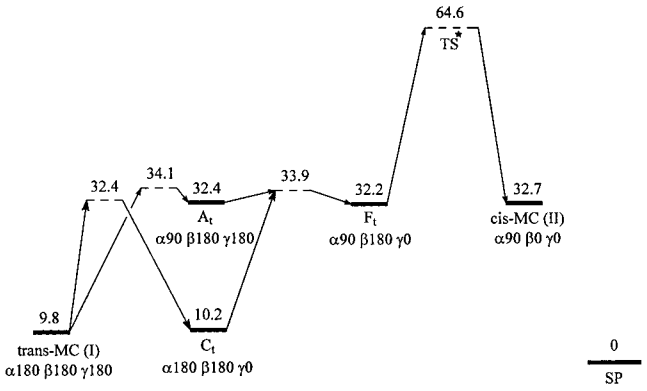

Figure 10. Potential energy diagram (kcal/mol) depicting the dihedral bond rotations (Tables 2−4) that define the lowest energy pathways (→) in the thermal reversion of *trans*-MC (I) to *cis*-MC (II), to SP, with dashed plateaus (- - -) indicating highest energy conformers.

interactions will increase the barrier in the conversion of *trans*-MC to *cis*-MC (Figure 8a), since there are specific steric requirements associated with this process which will experience steric encumbrance. In the case of MC-I, there is no evidence of repulsion between the methyl group and the phenolate moiety hindering cyclization.

The magnitude of the electrostatic repulsion will be dependent on the charge density of the interacting groups. As shown in Figure 9, the charge density on the SO_3^- moiety is much greater than that on COOH. The ligand end-group with the higher electron density will cause greater electrostatic repulsion during conversion of *trans*-MC to *cis*-MC and hence a larger barrier to rotation. This is in accord with the relative rate constants for reversion of MC-II and III, k_{obs}(MC-II) > k_{obs}(MC-III), indicative of larger electrostatic repulsions occurring between the phenolate and the sulfonate ligand in the MC-III system.

4. Molecular Modeling. As stated in the Introduction, the SP ⇌ MC thermal interconversion includes a further species, the *cis*-MC form, as a transient intermediate.[9] Inspection of molecular models shows that ring closure will be facilitated from the *cis*-MC as opposed to from the *trans*-MC form.

Initially, calculations were performed on three species: *trans*-MC, *cis*-MC, and SP. With SP normalized at 0 kcal/mol, the calculated ΔH_f values of *cis*-MC (II) and *trans*-MC (I) were 32.7 and 9.8 kcal/mol, respectively, as shown in Figure 10. This is in accord with the experimentally observed thermal reversion occurring from MC → SP, the thermodynamically more stable species.

In the stepwise procedure (Figure 3, path a), the transformation from *trans*-MC (I) to *cis*-MC (II) must entail a minimum of three elementary steps, i.e., rotations about the dihedral angles α, β, and γ: $\alpha 180 \rightarrow 90$, $\beta 180 \rightarrow 0$, and $\gamma 180 \rightarrow 0$ (Figure 2). ΔH_f values were calculated at 15° intervals of the dihedral angles. The energy maxima in Figure 11 correspond to the highest energy conformations of the dihedral rotation.

The data in Table 2 show that the barrier on going from *trans*-MC (I) to conformer $\mathbf{B_c}$ is the highest of three rotations (α, β, γ), and hence β rotation at this stage can be eliminated. The

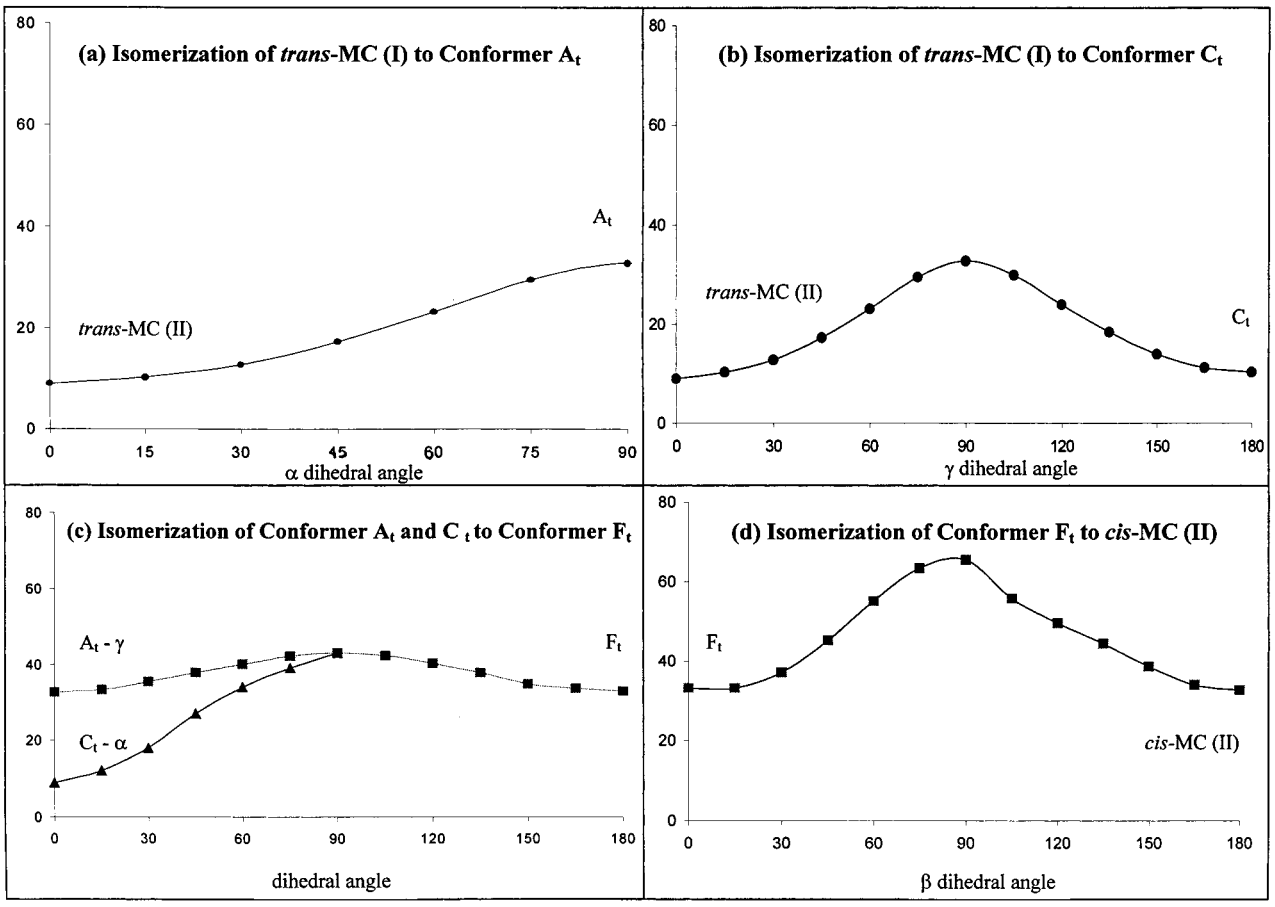

Figure 11. Potential energy diagrams depicting the lowest energy pathways for MC-I to SP: (a) *trans*-MC (I) → $\mathbf{A_t}$; (b) *trans*-MC (I) → $\mathbf{C_t}$; (c) $\mathbf{A_t}$ and $\mathbf{C_t}$ → $\mathbf{F_t}$; (d) $\mathbf{F_t}$ → *cis*-MC (II).

barriers for α and γ bond rotation to form conformers $\mathbf{A_t}$ and $\mathbf{C_t}$ differ only by 1.7 kcal/mol, suggesting that both pathways can occur due to the minimal energy difference. This is confirmed by dynamic NMR studies of the open-form MCs of spironaphthoxazines and 3*H*-naphthopyrans in solution which showed that, along with the *trans*-MC (I) form, another MC species was detected and was identified as corresponding to the $\mathbf{C_t}$ conformer.[8] This demonstrates that an equilibrium is established between *trans*-MC (I) and conformer $\mathbf{C_t}$, which is in accord with our calculations.

Barriers to rotation for both the α and γ dihedrals are large (Figure 11a,b) because merocyanines possess the characteristics of *vinylogous amides*, due to the dipolar nature of the conjugated double bonds that separate the donor and acceptor atoms.[24] Thus, even though the molecule is described structurally as having alternating single and double bonds, the bond orders are actually hybrids, which accounts for the appreciable rotational barriers associated with the α and γ dihedrals.

On proceeding from the $\mathbf{A_t}$ and $\mathbf{C_t}$ conformers after the first bond rotation, rotation of the β dihedrals can again be excluded since this implies a *trans* → *cis* isomerization about the formal double bond, i.e., the energy required to uncouple the π-bond in a *trans* geometry and re-form the *cis* geometry. Hence, the energetically favorable second rotations of conformers $\mathbf{A_t}$ and $\mathbf{C_t}$ will be those of the γ and α dihedrals, respectively, to form conformer $\mathbf{F_t}$ (Figure 11c). Finally, rotation of the β dihedral in conformer $\mathbf{F_t}$ leads to *cis*-MC (II). The process entails *trans* → *cis* isomerization and is associated with a large barrier to rotation, 32.4 kcal/mol (Figure 11e).

Lowest Energy Pathway. In a previous computational study by Abe et al., semiempirical calculations were used to investigate the interconversion of the four planar *trans*-MC isomers of 6-nitro-BIPS (α = 0, 180, β = 180, γ = 0, 180).[7] Barriers to rotation between the conformers were calculated to determine the sequence of dihedral rotations occurring in the overall thermal reversion of MC → SP. The calculations showed that three rotational isomers were involved in the thermal reversion process to SP: α180, β180, γ180 → α180, β180, γ0 → α0, β180, γ180 → SP. The potential energy diagrams for these processes showed no discontinuities. The barriers for the two rotations were 27 and 22 kcal/mol, while the cyclization to form SP had a barrier of 18 kcal/mol. Thus, the calculations of Abe et al. considered the cyclization from the *trans*-MC form to SP to occur directly, without the intermediacy of the *cis*-MC form.

The computations performed in the present work, in contrast, include the *cis*-MC form on the reaction pathway, as well as *trans*-MC forms. The necessity to include a *cis*-MC form is based on experimental results of (a) transient pico- and nanosecond spectroscopy[9] and (b) ligand/metal−ion complexation of bidentate MCs that traps the *cis*-MC form.[25] In these works, the *cis*-MC form has been detected as a transient intermediate in the photocoloration process, in accord with the *cis*-MC form being a well on the potential energy surface. Inclusion in the present work of the *cis*-MC form computationally has allowed the lowest energy pathway to be calculated on the basis of the three dihedral rotations required to transform *trans*-MC (I) to *cis*-MC (II) (Figure 2). It should be noted, however, that the actual values of calculated rotational barriers and the enthalpies may not be quantitative; nevertheless, they lead to improved understanding of the processes that take place and enable one to determine the rotational barrier with the highest energy.

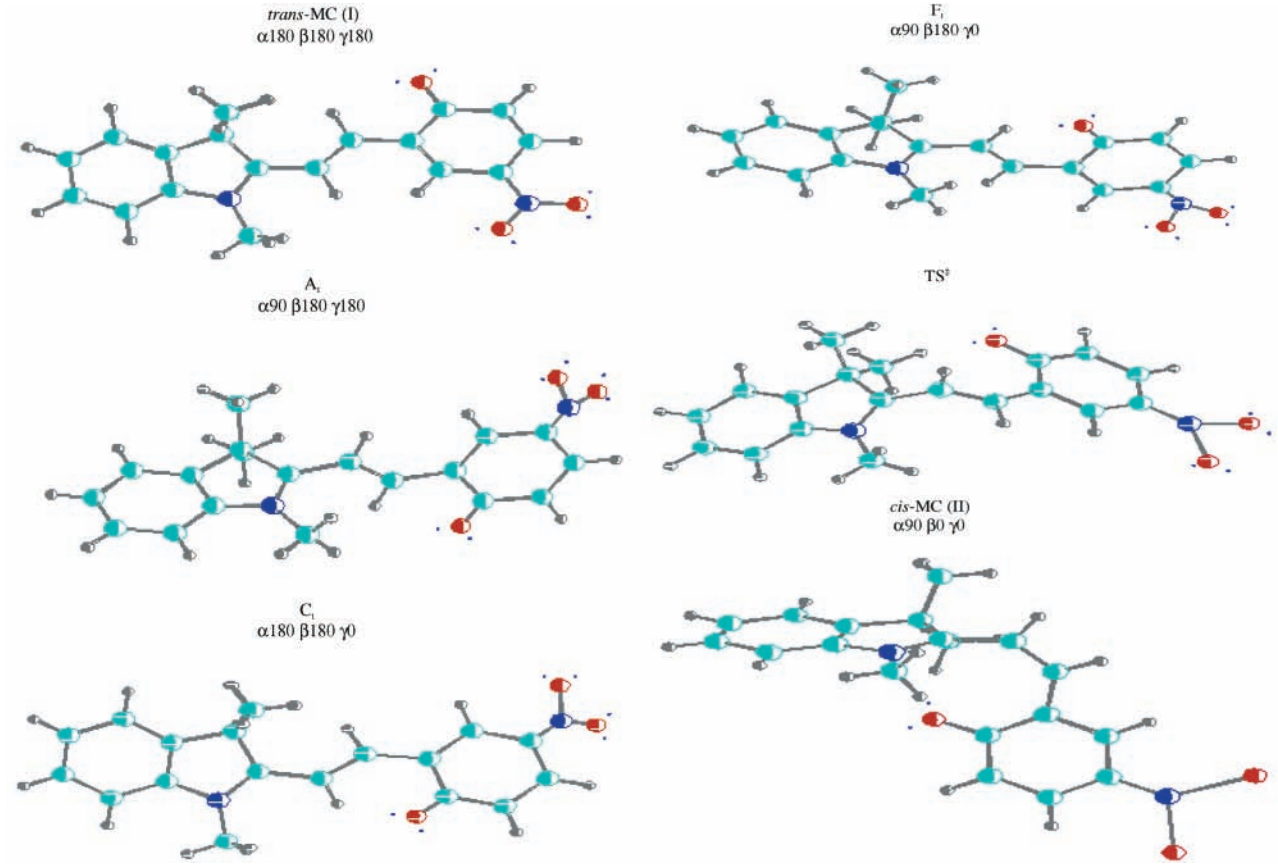

Figure 12. Calculated structures of conformational isomers for the lowest energy pathway in the conversion of *trans*-MC (I) → *cis*-MC (II).

Figure 12 shows the key structures involved in the conversion of *trans*-MC (I) → *cis*-MC (II) on the basis of the rotational barriers enumerated in Tables 2-4 and depicted graphically in Figure 11. The reaction coordinate diagram in Figure 10 shows clearly that the RDS in the *trans*-MC (I) → *cis*-MC (II) conversion corresponds to *trans*−*cis* isomerization of *trans* conformer $\mathbf{F_t}$ to *cis*-MC (II) and is associated with an energy barrier of 32.4 kcal/mol. Furthermore, the molecular modeling calculations have shown that the RDS of any plausible stepwise path in the conversion of *trans*-MC (I) to *cis*-MC (II) corresponds to dihedral rotation about the central β bond. There is a formal analogy to *cis/trans* isomerization of stilbene[26] and azobenzene,[27] where the process involves π-bond rupture and the highest energy TS has the benzene rings perpendicular to one another.

Conclusions

The effect of N-indolino substituents on the thermal reversion process, MC → SP, of a series of MCs has been examined via solvent effects on the absorption maxima and the thermal reversion rates, as well as through semiempirical calculations. For the N-functionalized MCs, the solvent effects on the reaction rates have shown that two major factors are influencing the thermal reversion process by affecting the rate-determining step of the reaction. The first is electrostatic and steric repulsions between the aryloxide moiety and the N-ligand, while the second is the extent of double-bond character of the central C−C bond. The interactions of the N-ligand and the aryloxide moiety are independent of solvent, whereas the bond order of the central bond is solvent-dependent. In nonpolar solvents, electrostatic and steric repulsions constitute the major influence on the RDS because the quinoid nature of the MC is associated with essentially single bond character of the central bond. However, on increasing the solvent polarity, the central bond order increases significantly, approaching 2, and the rotational barrier increases and eventually supplants ligand/phenoxide interaction as the chief factor responsible for hindering the thermal reversion rate. Accordingly, on increasing the solvent polarity beyond that of acetone, the kinetic behavior of all MCs in this study becomes similar, i.e., a progressive decrease of the observed rate constant for thermal reversion. The reaction mechanism in solvents of higher polarity is independent of the nature of the N-functionality since the primary contribution to the energy barrier in the rate-determining step is the central bond order, as dictated by the solvent. This was further demonstrated through dissecting the thermal reversion process into a series of dihedral rotations via semiempirical PM3 calculations, which have confirmed that the RDS of the thermal reversion mechanism is the *trans/cis* isomerization about the central bond.

Acknowledgment. Support of this research by a grant from the Natural Sciences and Engineering Research Council of Canada is gratefully acknowledged.

Supporting Information Available: Reaction coordinate analysis of the lowest energy pathway for the thermal reversion of *trans*-MC (I) to *cis*-MC (II). This material is available free of charge via the Internet at http://pubs.acs.org.

References and Notes

(1) (a) Hirshberg, Y. *New Scientist* **1960**, *7*, 1243. (b) Hirshberg, Y. *J. Am. Chem. Soc.* **1956**, *78*, 2304.

(2) (a) Crano, J. C., Guglielmetti, R. J., Eds. *Organic Photochromic and Thermochromic Compounds*; Topics in Applied Chemistry; Kluwer Academic/Plenum: New York, 1999; Vols. 1 and 2. (b) Dürr, H., Bouas Laurent, H., Eds. *Photochromism, Molecules and Systems in Studies in Organic Chemistry*; Elsevier: Amsterdam, 1990; Vol. 40. (c) Brown, G.

H., Ed. Photochromism. In *Techniques of Chemistry*, 3rd ed.; Wiley-Interscience: New York, 1971.

(3) Feringa, B. L.; Lager, W. F.; DeLange, B. *Tetrahedron* **1993**, *49*, 8267.

(4) (a) Berkovic, G.; Krongauz, V.; Weiss, V. *Chem. Rev*. **2000**, *100*, 1741. (b) Kawata, S.; Kawata, Y. *Chem. Rev*. **2000**, *100*, 1777.

(5) (a) Dvornikov, A. S.; Malkin, J.; Rentzepis, P. M. *J. Phys. Chem*. **1994**, *98*, 6746. (b) Dvornikov, A. S.; Esener, S.; Rentzepis, P. M. 3-Dimensional Optical Storage Memory by Means of Two-Photon Interaction. In *Optical Computing*; Lee, S. H., Jahns, J., Eds.; Wiley: New York, 1993; p 287. (c) Parthenopoulos, D. A.; Rentzepis, P. M. *J. Appl. Phys*. **1990**, *68*, 814. (d) Parthenopoulos, D. A.; Rentzepis, P. M. *Science* **1989**, *245*, 843.

(6) Wojtyk, J. T. C.; Kazmaier, P. M.; Buncel, E. *J. Chem. Soc., Chem. Commun*. **1998**, 1703.

(7) Abe, Y.; Nakao, R.; Horii, T.; Okada, S.; Irie, M. *J. Photochem. Photobiol. A: Chem*. **1996**, *95*, 209.

(8) (a) Delbaere, S.; Bochu, C.; Azaroul, N.; Buntinx, G.; Vermeersch, G. *J. Chem. Soc., Perkin Trans. 2* **1997**, 1499. (b) Delbaere, S.; Luccioni-Houze, B.; Bochu, C.; Teral, Y.; Campredon, M.; Vermeesch, G. *J. Chem. Soc., Perkin Trans. 2* **1998**, 1153.

(9) (a) Gorner, H. *Chem. Phys. Lett*. **1998**, *282*, 381. (b) Gorner, H. *Chem. Phys*. **1997**, *222*, 315. (c) Bohne, C.; Fan, M. G.; Li, Z. H.; Laing, Y. C.; Lusztyk, J.; Scaiano, J. C. *J. Photochem. Photobiol. A: Chem*. **1992**, *66*, 79.

(10) (a) Malatesta, A.; Neri, C.; Wis, M. L.; Montanari, L.; Millini, R. *J. Am. Chem. Soc*. **1997**, *119*, 3451. (b) Kawanishi, Y.; Seki, K.; Tamaki, T.; Sakuragi, M.; Suzuki. Y. *J. Photochem. Photobiol. A: Chem*. **1997**, *109*, 237. (c) Sueshi Y.; Ohcho, M.; Nishimura, N. *Bull. Chem. Soc. Jpn*. **1985**, *58*, 2608. (d) Ollis, W. O.; Ormand, K. L.; Sutherland, I. O. *Chem. Commun*. **1968**, 1697.

(11) Namba, K.; Suzuki, S. *Bull. Chem. Soc. Jpn*. **1975**, *48*, 1323.

(12) Perrin, D. W.; Armarego, W. L. F. *Purification of Laboratory Chemicals*, 3rd ed.; Pergamon Press: Toronto, 1988.

(13) Stewart, J. J. P. *J. Comput. Chem*. **1998**, *10*, 209.

(14) Spartan 3.0 Computational Software, Wavefunction, Inc., Irvine, CA, 1993.

(15) Keum, S.-R.; Hur, M.-S.; Kazmaier, P. M.; Buncel, E. *Can. J. Chem*. **1991**, *69*, 940.

(16) (a) More-O'Ferrall, R. A. *J. Chem. Soc. B* **1970**, 274. (b) Jencks, D. A.; Jencks, W. P. *J. Am. Chem. Soc*. **1977**, *99*, 7848.

(17) Dähne, S. *Science* **1978**, *199*, 287.

(18) (a) Dimroth, K.; Reichardt, C.; Siepmann, T.; Bohlmann, F. *Liebigs Ann. Chem*. **1963**, *661*, 1. (b) Reichardt, C. *Liebigs Ann. Chem*. **1971**, *752*, 64.

(19) Rosenthal, I.; Peretz, P.; Muszkat, K. A. *J. Phys. Chem*. **1979**, *83*, 351.

(20) Swansburg, S.; Buncel, E.; Lemieux, R. P. *J. Am. Chem. Soc*. **2000**, *122*, 6594.

(21) (a) Dürr, H. *Angew. Chem., Int. Ed. Engl*. **1989**, *28*, 413. (b) Dürr, H. *Angew. Chem*. **1989**, *101*, 427.

(22) (a) Ritchie, C. D. *Can. J. Chem*. **1986**, *64*, 2239. (b) Ritchie, C. D. *J. Am. Chem. Soc*. **1983**, *105*, 3573.

(23) (a) Hoz, S.; Speizman, D. *J. Org. Chem*. **1983**, *48*, 904. (b) Hoz, S. *Acc. Chem. Res*. **1993**, *26*, 69. (c) Hoz, S.; Gross, Z.; Speizman, D. *J. Chem. Soc., Perkin Trans. 2* **1985**, 1143.

(24) (a) Abdel-Hakim, S. T.; Abdel-Kader, M. H.; Steiner, U. E. *J. Phys Chem*. **1998**, *92*, 4325. (b) Gao, J.; Alhambra, C. *J. Am. Chem. Soc*. **1997**, *119*, 2962.

(25) (a) Gorner, H.; Chibisov, A. K. *J. Chem. Soc., Faraday Trans*. **1998**, *94*, 2557. (b) Chibisov, A. K.; Gorner, H. *Chem. Phys*. **1998**, *237*, 425.

(26) Gorner, H.; Kuhn, H. J. *Adv. Photochem*. **1995**, *19*, 1.

(27) Beveridge, D. L.; Jaffe, H. H. *J. Am. Chem. Soc*. **1966**, *88*, 1948.